*Structural Engineering and Mechanics, Vol. 45, No. 6 (2013) 759-777* 
DOI: http://dx.doi.org/10.12989/sem.2013.45.6.759

# A topology optimization method for multiple load cases and constraints based on element independent nodal density

Jijun Yi[1,2], Jianhua Rong[*2], Tao Zeng[1] and X. Huang[3]

[1]*School of Mechanical and Electrical Engineering, Central South University, Changsha 410083, China*
[2]*School of Automobile and Mechanical Engineering, Changsha University of Science and Technology, Changsha 410004, China*
[3]*School of Civil, Environmental and Chemical Engineering, RMIT University, GPO Box 2476, Melbourne3001, Australia*

*(Received June 28, 2012, Revised December 26, 2012, Accepted February 19, 2013)*

**Abstract.** In this paper, a topology optimization method based on the element independent nodal density (EIND) is developed for continuum solids with multiple load cases and multiple constraints. The optimization problem is formulated as minimizing the volume subject to displacement constraints. Nodal densities of the finite element mesh are used as the design variables. The nodal densities are interpolated into any point in the design domain by the Shepard interpolation scheme and the Heaviside function. Without using additional constraints (such as the filtering technique), mesh-independent, checkerboard-free, distinct optimal topology can be obtained. Adopting the rational approximation for material properties (RAMP), the topology optimization procedure is implemented using a solid isotropic material with penalization (SIMP) method and a dual programming optimization algorithm. The computational efficiency is greatly improved by multithread parallel computing with OpenMP to run parallel programs for the shared-memory model of parallel computation. Finally, several examples are presented to demonstrate the effectiveness of the developed techniques.

**Keywords:** topology optimization; element independent nodal density; Shepard interpolation scheme; multiple load cases; multiple constraints; parallel computation

## 1. Introduction

Structural optimization seeks to achieve the best performance for a structure while satisfying various constraints such as given displacements. The types of structural optimization may be classified into three categories, i.e., size, shape and topology optimization (Lee 2007, Lee and Park 2011). Compared with other types of structural optimization, topology optimization of continuum structures is the most challenging technically but the most rewarding economically (Lee *et al.* 2012).

Topology optimization can greatly enhance the performance of structures for many engineering application. Starting with the landmark paper of Bendsøe and Kikuchi (1988), numerical methods

*Corresponding author, Professor, E-mail: Rongjhua@yahoo.com.cn

for topology optimization of continuum structures have been investigated extensively. Most of these methods are based on finite element analysis (FEA) where the design domain is divided into a fine mesh of finite elements. The most popular methods for topology optimization include the homogenization design method (HDM) (Bendsøe and Kikuchi 1988), the solid isotropic material with penalty (SIMP) method (Bendsoe 1989, Rozvany *et al.* 1992, Yang and Chuang 1994, Rozvany 2001), the evolutionary structural optimization (BESO) method (Xie and Steven 1993, Xie and Steven 1997) and its later version, the bi-directional ESO (Huang and Xie 2010), and the level set method (Sethian and Wiegmann 2000, Wang *et al.* 2003, Rong and Liang 2008).

In these methods, the elements within the design domain are used for discretizing both the material distribution and the displacement fields. Elemental densities which are assumed uniform within each element are taken as design variables. The element-wise topology optimization performed by these methods exhibits various numerical problems, such as grey-scale, checkerboard pattern and mesh-dependency.

Diaz and Sigmund (1995) discussed the reasons for the formation of checkerboard patterns and demonstrated that solid and void materials arranged in element-wise checkerboard patterns are given artificial stiffness. Sigmund and Petersson (1998) discussed many of the numerical instability problems encountered in topology optimization. The usage of higher order finite elements, the imposition of a perimeter constraint and spatial filtering techniques are proved to be effective in suppressing the numerical instabilities. Filtering techniques such those proposed by Sigmund and Petersson (1998), Swan and Kosaka (1997), Huang and Xie (2007) are widely used due to its simplicity. However, the resulting optimal topologies highly depended on the filtering characteristics.

In order to overcome the numerical instability and to ensure a clear and smooth optimal topology, a topology optimization method based on nodal design variables is developed. An essential issue for a topology optimization approach is how to construct the material density field using the continuous values of the density design variables. In some studies, conventional displacement shape functions have been used to interpolate the nodal density values to the element-wise material density distribution (Carbonari *et al.* 2004, Matsui and Terada 2004, Rahmatalla and Swan 2004, Paulino and Le 2009). However, these approaches are restricted to the case of bi-linear elements, since higher-order finite element (e.g., 8-node quadrilateral element) shape functions possess no range-restricted property. Poulsen (2002) used wavelet basis functions to interpolate the nodal design variables and achieved designs which are nearly free of checkerboard and one-node connected hinge.

In the above mentioned interpolation scheme, the nodal design variables are converted to element-wise constant densities when evaluating elemental stiffness matrices. The approaches can successfully achieve optimal topologies with non-smooth contour. However, Topology optimization methods based on continuous distribution of material densities can overcome checkerboard patterns and obtain smooth topology by virtue of the continuous approximation. The basic idea is to construct the continuous density field from the design variables within the whole design domain rather than within each element through the interpolation scheme. Jog and Haber (1996) found both the Q4/U and Q4/Q4 implementations to be unstable, even with the Q9/U and Q8/U implementations, and introduced the interpolation with control parameters. Matsui and Terada (2004) presented a so-called CAMD (continuous approximation of material distribution) model into the homogenization topology optimization method. Rahmatalla and Swan (2004) proposed a Q4/Q4 implementation of the SIMP method, in which the checkerboard patterns can be effectively avoided. Meanwhile, a new problem, namely the so-called “islanding” phenomenon,

was observed. Kang and Wang (2011) presented a non-local density interpolation method so that the "islanding" phenomenon can be avoided.

In many topology optimization references, the compliance is taken as the objective function, and structural volume is treated as a constraint. But in engineering practice, the final volume is often unpredictable. Most real structures are subjected to different loads at different times. This is referred to as multiple load cases. An optimal topology for multiple loads is much safer if the loading conditions are not precisely known or subject to change. So a topology optimization method of the element independent nodal design variables is developed for continuum solids with multiple load cases and multiple constraints in this paper. This paper applies the developed method to the topology optimization of continuum solids with the objective of minimizing the volume subject to displacement constraints.

## 2. Nodal design variables and the interpolation scheme

In continuous formulations of topology optimization problems, elemental densities are defined as the design variables and a penalty is applied to the design variable field, i.e. as in the so-called "power law approach" or density distribution method. However, element independent nodal densities are taken as the design variables of the topology optimization problem in this paper. The densities are distributed as point densities within the whole design domain. Element density is not constant so that the density field must be determined to obtain structural stiffness etc. properties. Here, Shepard interpolation scheme is adopted to obtain the density field. Thus, the relative density of any point must be interpolated by an interpolation scheme.

### *2.1 The influence domain and node identifications inside it*

In order to determine the relative density of any point $x$ in the design domain, the influence domain of this point and corresponding nodes need to be determined. As proposed by Guest *et al.* (2004), Kang and Wang (2011), the scale parameter $r_{min}$ is set to identify the nodes that influence the density of point $x$, as shown in Fig. 1(a). Nodes are included in the influence domain if they are located within a distance $r_{min}$ of the point $x$. This can be visualized by drawing a circle (or sphere in 3D cases) of radius $r_{min}$ centered at the point $x$, thus generating the circular (or spherical) sub-domain $\Omega^x$. Nodes located inside $\Omega^x$ contribute to the computation of density $\rho(x)$ of point $x$. As the mesh is refined, $r_{min}$ and consequently $\Omega^x$ do not change. The only difference between the two meshes is the number of nodes located inside $\Omega^x$ and included in the interpolation function, as shown in Fig. 1(b). This is essential to generating mesh-independent solutions.

### *2.2 Shepard interpolation scheme*

Interpolation will provide continuum of density field and mesh-independent solutions, so as to alleviate numerical instability and checkerboard effects (Diaz and Sigmund 1995). In implementing continuum structural topology optimization formulations, many functions are available to interpolate nodal density onto the points inside the element space—for example, the standard $C^0$ shape functions used in the finite element method. However, each node's shape function influences only the elements connected to that node. Mesh-independent solutions cannot be obtained if interpolation functions are influenced by mesh size. The scale parameter $r_{min}$ should

be based on a physical length scale which does not change with mesh refinement.

In this study, Shepard (Shepard 1968, Brodlie *et al.* 2005, Kang and Wang 2011) interpolation method is used to achieve the mesh-independency effect. Let $\rho_i (i = 1, 2, \ldots, n)$ denote a set of density of nodes inside $\Omega^x$ centered at the point $x = (X, Y, Z)$, where $(X, Y, Z)$ define the location of the point $x$ in the Cartesian coordinate system. Thus the relative density at point $x$ is calculated by the nodal densities inside the influence domain $\Omega^x$ with Shepard interpolation method as.

$$\mu(x) = \begin{cases} \sum_{i \in S_x} N_i(x)\rho_i & (x \neq x_i) \\ \rho_i & (x = x_i) \end{cases} \tag{1}$$

$$\rho(x) = 1 - e^{-\beta\mu} + \mu e^{-\beta} \tag{2}$$

where $S_x$ is the set of design variables whose corresponding nodes are located within the influence domain $\Omega^x$ of point $x$, and $\rho_i$ is the density value of the $i$th node. $x_i$ is the position of the point associated with the $i$th node. The parameter $\beta$ dictates the curvature of Eq. (2). Eq. (2) is linear when $\beta = 0$, and approaches the Heaviside step function as $\beta$ approaches infinity (Guest *et al.* 2004). In this paper, $\beta = 5$ is set. The white-black solution can be obtained with Eq. (2). The corresponding interpolation function $N_i(x)$ is defined as

$$N_i(x) = \frac{R_i(x)}{\sum_{i=1}^{n} R_i(x)} \quad (i = 1, 2, \ldots, n) \tag{3}$$

where $R_i(x) = 1/r_i(x)$ and $r_i(x) = |x - x_i|_2$ being the Euclidean distance from the points $x$ to $x_i$. $n$ is the total number of nodes inside the influence domain $\Omega^x$.

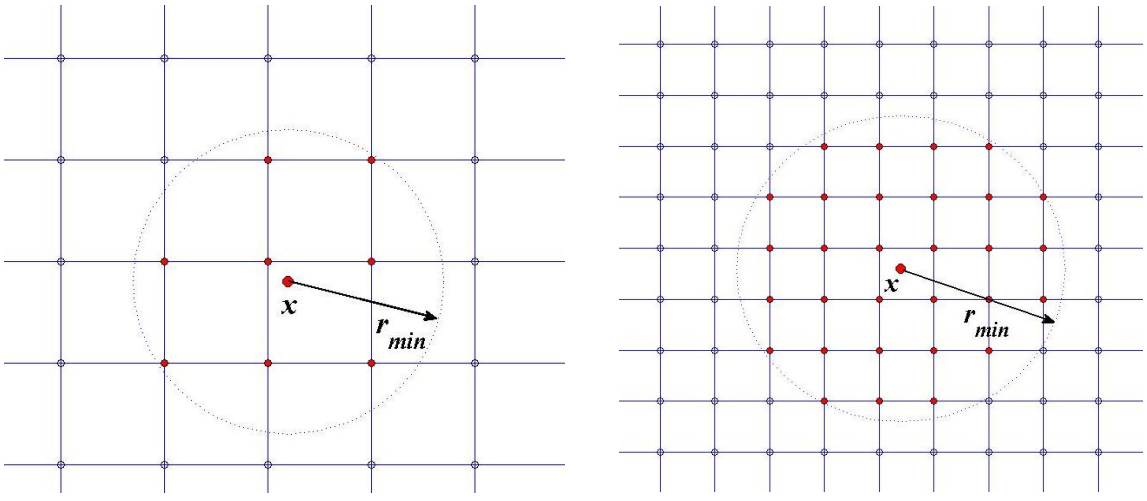


(a) (b)

Fig. 1 The same $r_{min}$: (a) The influence domain of the point $x$. (b) The influence domain of the point $x$ when the mesh is refined

In the method using element independent nodal density variables, the density in the element space is not constant, and the global density field of the structure has $C^0$ continuity. It is also easy to know that $0 \le \rho^x \le 1$ holds if $0 \le \rho_i \le 1 \ \ (i \in S_x)$ from the bounded property of Shepard interpolation. Moreover, the property $N_i(x) \ge 0$ guarantees that the derivative of the density with respect to the design variable will be always non-negative. This property is essential for ensuring a correct searching direction in seeking the optimal material distribution by a gradient-based algorithm.

## 3. Formulation of topology optimization and numerical implementation

In the SIMP method (Bendsoe 1989, Yang and Chuang 1994, Rozvany 2001, Kang and Wang 2011), the discrete topological variables $\rho_i$ that only take value 0 or 1 are relaxed by continuous topological variables between 0 and 1. Consequently, the difficulty of the discrete optimization problem is avoided by penalization. Similarly, the rational approximation for material properties (RAMP), which was proposed by Stolpe and Svanberg (2001), is adopted and stated as

$$f\ (\rho(x)) = \frac{\rho(x)}{1+q\left(1-\rho(x)\right)} \tag{4}$$

where $q$ is the penalization factor. In this paper, $q$ = 5 is used so that the intermediate density approaches either 0 (void) or 1(solid). The relation between the Young's modulus and the material density at point $x$ is expressed by

$$E\left(x\right) = f\left(\rho(x)\right)E^0 \tag{5}$$

where $E^0$ is Young's modulus of the fully solid material.

The function $f(\rho(x))$ has the following properties:

$$f(\rho(x)) = 0 \qquad as\ \ \rho(x) \to 0_+$$

$$d\ f(\rho(x)) / d\ \rho(x) = \frac{1}{1+q} \ne 0 \quad as\ \ \rho(x) \to 0_+$$

The actual volume of an element is given by

$$V_i = \int_{V_i^0} \rho(x) dV \tag{6}$$

where $V_i^0$ is the original volume of the $i$th element.

### *3.1 Optimal model*

Topology optimization of continuum structures aims to optimize the material densities which are considered as design variables in the design domain. In this study, minimum volume with the reference domain $\Omega$ in $R^2$ or $R^3$ is considered while satisfying displacement constraints. The topology optimization problem can be stated as

$$\begin{cases} \min\ V = \sum_{i=1}^{N_{el}} V_i \\ s.t.\quad \left|u_j^f\right| \le U_j \quad (j = 1,\cdots,J;\ f = 1,2,\cdots,L) \\ \qquad \underline{\rho_i} \le \rho_i \le 1 \qquad\qquad (i_q = 1,2,\cdots,N_{nod}) \end{cases} \tag{7}$$

where $V$ is the structural volume being optimized, $V_i$ is the volume of the $i$th element, $N_{el}$ is the number of all elements. $u_j^f$ is the displacement of the $j$th degree of freedom of the structure under the $f$th load case, $U_j$ is its constraint limit. $J$ is the number of the displacement constraints for each load case, $L$ is the number of the load cases acting on the structure. $\rho_i$ is the density of $i$th node, $\underline{\rho_i}$ is its lower limit. $N_{nod}$ is the total number of the nodes in the design domain. Here the small positive lower bound $\underline{\rho_i} = 0.0001$ is set to avoid the singularity of the problem.

### 3.2 Sensitivity analysis

A number of numerical methods are available for optimum search. Here, SQP (Sequential Quadratic Programming) is used. The solution of the gradient-based optimization problem requires the computation of sensitivities of the objective function and the constraints.

In a finite element analysis, the static behavior of a structure for any load case can be expressed by the stiffness equation as

$$\mathbf{Ku} = \mathbf{F} \tag{8}$$

where $\mathbf{K}$ is the global stiffness matrix of a structure being optimized and, $\mathbf{u}$ and $\mathbf{F}$ are the global nodal displacement and nodal force vectors respectively.

It is assumed that the nodal density $\rho_i$ has no effect on the applied load vector. Assuming $t_i = 1/\rho_i$, the partial derivative of the displacement vector with respect to $t_i$is calculated from Eq. (8) as

$$\frac{\partial \mathbf{u}}{\partial t_i} = -\mathbf{K}^{-1}\frac{\partial \mathbf{K}}{\partial t_i}\mathbf{u} \tag{9}$$

The sensitivity of the $j$th displacement can be calculated using the adjoint method (Bendsoe and Sigmund 2003). To find the partial derivative of $u_j$ with respect to $t_i$, a virtual force vector $\mathbf{F}_j$ in which only the $j$th component is equal to unity and the others are equal to zero is introduced. Multiplying Eq. (9) by $\mathbf{F}_j^T$, the following equation can be obtained

$$\begin{aligned} \frac{\partial u_j}{\partial t_i} &= -\mathbf{u}_j^T\frac{\partial \mathbf{K}}{\partial t_i}\mathbf{u} \\ &= -\sum_{e=1}^{N_{con}} \mathbf{u}_j^{eT}\frac{\partial \mathbf{K}^e}{\partial t_i}\mathbf{u}^e \end{aligned} \tag{10}$$

$$\frac{\partial \mathbf{K}^e}{\partial t_i} = \frac{\partial \mathbf{K}^e}{\partial \rho_i}\frac{\partial \rho_i}{\partial t_i} = -\frac{1}{t_i^2}\frac{\partial \mathbf{K}^e}{\partial \rho_i} \tag{11}$$

where $\mathbf{u}_j$ is the displacement vector due to the unit virtual force $\mathbf{F}_j$, And $\mathbf{u}^e$ and $\mathbf{u}_j^e$ are the element displacement vectors containing the entries of $\mathbf{u}$ and $\mathbf{u}_j$, respectively, which are related to the $e$th element. $N_{con}$ is the number of element influenced by $\rho_i$. $\mathbf{K}^e$ is the element stiffness matrix of the $e$th element.

The sensitivity of the displacement requires the computation of the sensitivity of the stiffness matrix with respect to the design variable. The derivative of the elemental stiffness matrix with respect to the design variable is expressed by

$$\begin{aligned}\mathbf{K}^e &= \int_{\Omega_e} \mathbf{B}^T \mathbf{D}(\rho)\mathbf{B}\, d\Omega_e \\ &= \int_{\Omega_e} f_E(\rho)\mathbf{B}^T \mathbf{D}_0 \mathbf{B}\, d\Omega_e\end{aligned} \tag{12}$$

$$\frac{\partial \mathbf{K}^e}{\partial \rho_i} = \int_{\Omega_e} \frac{\partial f\ (\rho(x))}{\partial \rho_i} \mathbf{B}^T \mathbf{D}_0 \mathbf{B}\, d\Omega_e \tag{13}$$

$$\frac{\partial f\left(\rho(x)\right)}{\partial \rho_i} = \frac{\partial f\left(\rho_j^e\right)}{\partial \rho(x)} \frac{\partial \rho(x)}{\partial \mu_i} \frac{\partial \mu}{\partial \rho_i} = \frac{(1+q)}{\left((1-\rho(x))q+1\right)^2} N_{ji}\left(\beta e^{-\beta\mu} + e^{-\beta}\right) \tag{14}$$

where $\mathbf{B}$ is the conventional displacement-strain matrix and $\mathbf{D}_0$ corresponds to the constitutive matrix of the solid material.

For example, the formulation of the constitutive matrix for 3D isotropic solid structures is

$$\mathbf{D}(x) = \frac{E(x)(1-\mu)}{(1+\mu)(1-2\mu)} \begin{bmatrix} 1 & \frac{\mu}{1-\mu} & \frac{\mu}{1-\mu} & 0 & 0 & 0 \\ & 1 & \frac{\mu}{1-\mu} & 0 & 0 & 0 \\ & & 1 & 0 & 0 & 0 \\ & & & \frac{1-2\mu}{2(1-\mu)} & 0 & 0 \\ & \textit{symmetry} & & & \frac{1-2\mu}{2(1-\mu)} & 0 \\ & & & & & \frac{1-2\mu}{2(1-\mu)} \end{bmatrix} \tag{15}$$

The stiffness matrix integrand is evaluated at the Gauss points and the densities at these Gauss points are directly computed from the design variables using interpolation function. Numerical quadrature, such as Gaussian quadrature, is commonly reduced to the evaluation and summation of the stiffness integrand at specific Gauss points.

The sensitivity analysis of the objective function in Eq. (7) can be calculated similarly. The derivative of the total material volume with respect to the design variables can be computed by Gauss quadrature method over the influence domain. The elemental volume is

$$\begin{aligned} V_e &= \int_{\Omega_e} \rho(x) d\Omega_e \\ &= \int_{\Omega_e} \sum_{i \in S_x} N_i(x) \rho_i \, d\Omega_e \end{aligned} \tag{16}$$

and the total structural volume of the structure is

$$V = \sum_{e=1}^{N_{el}} V_e = \sum_{e=1}^{N_{el}} \int_{\Omega_e} \sum_{i \in S_x} N_i(x) \rho_i \, d\Omega_e \tag{17}$$

The derivative of $V$ with respect to the design variable is

$$\frac{\partial V}{\partial \rho_i} = \sum_{e=1}^{N_{el}} \int_{\Omega_e} N_i \, d\Omega_e \tag{18}$$

$$\frac{\partial V}{\partial t_i} = \frac{\partial V}{\partial \rho_i} \frac{\partial \rho_i}{\partial t_i} = -\frac{1}{\left(t_i\right)^2} \sum_{e \in S_x} \left( \int_{\Omega_e} N_i d\Omega_e \right) \tag{19}$$

### *3.3 Topology optimization with varying displacement limits*

The displacement constraints cannot be satisfied easily because the actual values of the displacements may far away from their constraint values. In order to make the approximation functions of displacement constraints in Eq. (7) hold true at each iteration process and make the optimum topology obtained be of good 0-1 distribution topology variable property at the same time, an equivalent optimization model (20) with varying displacement constraint limits is built. And these varying displacement constraint limits are of the function of design variable trust-regions.

$$\begin{cases} \min \; V = \sum_{e=1}^{N_{el}} \int_{\Omega_e} \rho d\Omega_e \\ s.t. \quad \left|u_j^f\right| \le U_j^{l\,f} \quad (j = 1, \cdots, J; \; f = 1, 2, \cdots, L; \quad l = 1, 2, \cdots) \\ \qquad \underline{\rho_i} \le \rho_i \le 1 \qquad (i = 1, 2, \cdots, N_{nod}) \end{cases} \tag{20}$$

where $U_j^{l\,f}$ is expressed as

$$\begin{aligned} U_j^{l\,f} = & \begin{cases} \left|u_j^{k\,f}\right| + min\left(\alpha \left|u_j^{k\,f}\right|, (U_j - \left|u_j^{k\,f}\right|)\right), & \left|u_j^{k\,f}\right| \le U_j \\ \left|u_j^{k\,f}\right| - min\left(\alpha \left|u_j^{k\,f}\right|, \left|U_j - \left|u_j^{k\,f}\right|\right|\right), & \left|u_j^{k\,f}\right| > U_j \end{cases} \\ & j = 1, \cdots, J; \quad l = 1, 2, \cdots \\ & f = 1, 2, \cdots, L \end{aligned} \tag{21}$$

where, $\alpha$ is a displacement limit changing factor. Typical values of $\alpha$ between 0.01 and 0.20 have

been used for displacement constraints in the example problems in this paper. $u_j^{kf}$ is the displacement of the *j*th degree of freedom of the structure under the *f*th load case at the *k*th iteration. $U_j^{lf}$ $(j=1,2,\cdots,J)$ are varied according to Eq. (21) at every iteration. It can be seen that the above approximate displacement constraints $U_j^{lf}$ gradually approach the original displacement constraints $U_j$.

The first-order series expansion for the displacement function $u_j$ at $t_i$ ($i$ = 1, 2, …, $N_{nod}$) can expressed as

$$u_j = u_j^k + \sum_{i=1}^{N_{nod}} (u_j)'_{t_i}\Big|_{t_i^k} (t_i - t_i^k) \tag{22}$$

Let $c\left(t_i^k\right) = \left.\dfrac{\partial u_j}{\partial t_i}\right|_{t_i^k}$

$$u_j = u_j^k - \sum_{i=1}^{N_{nod}} c\left(t_i^k\right) t_i^k + \sum_{i=1}^{N_{nod}} c\left(t_i^k\right) t \tag{23}$$

Thus, the *j*th displacement in the next iteration, $u_j^{k+1}$, can be estimated by the *j*th displacement in the current iteration.

Let $C_{ij}^f = c(t_i^k)sign(u_j^{kf})$ $(i=1,\ldots,N_{nod})$ and $A_i^f{}_j = c(t_i^k)t_i^k sign(u_j^{kf})$ $(i=1,\cdots,N_{nod})$,

Therefore, Eq. (20) can be transferred into Eq. (24)

$$\begin{cases} \min: \quad V = \sum_{e=1}^{N_{el}} \int_{\Omega_e} 1/t \, d\Omega_e \\ s.t. \quad \sum_{i=1}^{N_{nod}} C_i^f{}_j t_i \le \bar{U}_j^{lf} - u_j^{kf} sign(u_j^{kf}) + \sum_{i=1}^{N_{nod}} A_i^f{}_j \\ \qquad\qquad (j=1,\cdots,J;\ f=1,2,\cdots L; \quad l=1,2,\cdots) \\ \quad 1 \le t_i \le \bar{t}_i \qquad\qquad (i=1,2,\cdots,N_{nod}) \end{cases} \tag{24}$$

As the constant items in the objective function can be omitted, Eq. (24) is equivalent to Eq. (25)

$$\left.\begin{array}{l} find \quad t \in R^{N_{nod}} \\ \min: \quad \sum_{i=1}^{N_{nod}} \left(b_i (t_i)^2 + a_i t_i\right) \\ s.t. \quad \sum_{i=1}^{N_{nod}} C_i^f{}_j t_i \le \bar{U}_j^{lf} - u_j^{kf} sign(u_j^{kf}) + \sum_{i=1}^{N_{nod}} A_i^f{}_j \\ \quad 1 \le t_i \le \bar{t}_i \end{array}\right\} \tag{25}$$

here

$$a_i = \frac{-3}{\left(t_i^{(k)}\right)^2}\sum_{j=1}^{N_{el}}\left(\int_{\Omega_j} N_i\left(\beta e^{-\beta\mu}+e^{-\beta}\right)d\Omega_j\right)+\frac{1}{\left(t_i^{(k)}\right)^3}\sum_{j=1}^{N_{con}}\left(\int_{\Omega_j}\left(N_i\beta\right)^2 e^{-\beta\mu}d\Omega_j\right)$$

$$b_i = \frac{1}{\left(t_i^{(k)}\right)^3}\sum_{e=1}^{N_{con}}\left(\int_{\Omega_e} N_i\left(\beta e^{-\beta\mu}+e^{-\beta}\right)d\Omega_e\right)-\frac{1}{2\left(t_i^{(k)}\right)^4}\sum_{e=1}^{N_{con}}\left(\int_{\Omega_e}\left(N_i\beta\right)^2 e^{-\beta\mu}d\Omega_e\right)$$

The above optimization problem can be rewritten as the following dual optimization model (Beckers 1999, Rong *et al.* 2010).

$$\begin{cases}\max:\varphi(\boldsymbol{\lambda})\\ s.t.\quad \boldsymbol{\lambda}\geq 0\end{cases} \tag{26}$$

where $\boldsymbol{\lambda}$ are the Lagrange multipliers and $\varphi(\boldsymbol{\lambda})=\min_{1\leq t_i\leq \bar{t}_i, i=1,\cdots,N_{nod}}(L(\mathbf{t},\boldsymbol{\lambda}))$,

$$L(\mathbf{t},\boldsymbol{\lambda})=\sum_{i=1}^{N_{nod}}\left(b_i(t_i)^2+a_it_i\right)+\sum_{f=1}^{L}\sum_{j=1}^{J}\lambda_{((f-1)J+j)}(\sum_{i=1}^{N_{nod}}d_{ij}^f t_i-e_j^f)$$

$$d_{ij}^f = C_{ij}^f / \max_{i=1,\cdots,N_{nod}}(\left|C_{ij}^f\right|),\quad (f=1,2,\cdots,L;\ j=1,2,\cdots,J)$$

$$e_j^f=(\bar{U}_j^{lf}-u_j^{kf}sign(u_j^{kf})+\sum_{i=1}^{N_{nod}}A_{ij}^f)/\max_{i=1,2,\cdots,N_{nod}}(\left|C_{ij}^f\right|)$$

The first and second order partial derivatives of the objective function in Eq. (26) with respect to the Lagrange multipliers are derived as follows

$$\partial\phi(\boldsymbol{\lambda})/\partial\lambda_{((f_1-1)J+j)}\Big|_{\boldsymbol{\lambda}=\mathbf{0}}=\sum_{i=1}^{N_{nod}}d_{ij}^{f_1}t_i^*-e_j^{f_1}+\sum_{i=1}^{N_{nod}}(2b_it_i^*+a_i)\partial t_i^*/\partial\lambda_{((f_1-1)J+j)} \tag{27}$$

$$\begin{aligned}\partial^2\phi(\boldsymbol{\lambda})/(\partial\lambda_{((f_1-1)J+j)}\partial\lambda_{((f_2-1)J+k)})\Big|_{\boldsymbol{\lambda}=\mathbf{0}}&=\sum_{i=1}^{N_{nod}}2b_i\frac{\partial x_i^*}{\partial\lambda_{((f_2-1)J+k)}}\frac{\partial x_i^*}{\partial\lambda_{((f_1-1)J+j)}}+\\ &\sum_{i=1}^{N_{nod}}(2b_it_i^*+a_i)\partial^2t_i^*/\partial\lambda_{((f_1-1)J+j)}\partial\lambda_{((f_2-1)J+k)}+\\ &\sum_{i=1}^{N_{nod}}d_{ij}^{f_1}\frac{\partial t_i^*}{\partial\lambda_{((f_2-1)J+k)}}+\sum_{i=1}^{N_{nod}}d_{ik}^{f_2}\frac{\partial t_i^*}{\partial\lambda_{((f_1-1)J+j)}}\end{aligned} \tag{28}$$

The following equation can be obtained by the K-T condition and the Lagrange function.

$$\partial L(\mathbf{t},\boldsymbol{\lambda})/\partial x_i=2b_it_i^*+a_i+\sum_{f_1=1}^{L}\sum_{j=1}^{J}\lambda_{((f_1-1)J+j)}d_{ij}^{f_1}=\begin{cases}\leq 0 & t_i^*=\bar{t}_i\\ =0 & 1<t_i^*<\bar{t}\\ \geq 0 & t_i^*=1\end{cases} \tag{29}$$

Setting $I_a=\left\{i\,\middle|\,1<t_i^*<\bar{t}_i\quad (i=1,2,\cdots,N_{nod})\right\}$ as an active design variable set, from the second case in Eq. (29), the Eq. (30)can be derived directly

$$2b_i t_i^* + a_i + \sum_{f_1=1}^{L}\sum_{j=1}^{J} \lambda_{((f_1-1)J+j)} d_{ij}^{f_1} \equiv 0 \tag{30}$$

Therefore, the following equations can obtained

$$\partial t_i^* / \partial \lambda_{((f_1-1)J+j)} = -d_{ij}^{f_1} / (2b_i) \tag{31}$$

and

$$\partial^2 t_i^* / (\partial \lambda_{((f_1-1)J+j)} \partial \lambda_{((f_2-1)J+k)}) = 0 \tag{32}$$

Moreover, from the first and third cases in Eq. (29), the following equation can be obtained

$$\partial t_i^* / \partial \lambda_{((f_2-1)J+k)} = 0 \tag{33}$$

From Eqs. (27)-(28) and (30)-(33), the first and second order partial derivatives of the objective function with respect to Lagrange multipliers are simplified as follows

$$\partial \phi(\boldsymbol{\lambda}) / \partial \lambda_{((f_1-1)J+j)}\Big|_{\boldsymbol{\lambda}=\mathbf{0}} = \sum_{i=1}^{N_{nod}} d_{ij}^{f_1} t_i^* - e_j^{f_1} - \sum_{i\in I_a} (2b_i t_i^* + a_i) d_{ij}^{f_1} / (2b_i) \tag{34}$$

$$\partial^2 \phi(\boldsymbol{\lambda}) / (\partial \lambda_{((f_1-1)J+j)} \partial \lambda_{((f_2-1)J+k)})\Big|_{\boldsymbol{\lambda}=\mathbf{0}} = -\sum_{i\in I_a} d_{ij}^{f_1} d_{ik}^{f_2} / (2b_i) \tag{35}$$

When the constant items of the second order approximation of $\varphi(\boldsymbol{\lambda})$ are omitted, the following quadratic programming model dealing with Lagrange multipliers can be built.

$$\begin{cases} \min: \quad \dfrac{1}{2}\boldsymbol{\lambda}^T D \boldsymbol{\lambda} + H^T \boldsymbol{\lambda} \\ s.t. \quad \boldsymbol{\lambda} \geq 0 \end{cases} \tag{36}$$

where

$$\left.\begin{aligned} H_{((f_1-1)J+j)} &= -\sum_{i=1}^{N+1} d_{ij}^{f_1} t_i^* + e_j^{f_1} + \sum_{i\in I_a} (2b_i t_i^* + a_i) d_{ij}^{f_1} / (2b_i) \\ D_{((f_1-1)J+j),((f_2-1)J+k)} &= \sum_{i\in I_a} d_{ij}^{f_1} d_{ik}^{f_2} / (2b_i) \end{aligned}\right\} \tag{37}$$

In this paper, $t_i^* (i = 1, 2, \cdots, N_{nod})$ and $\boldsymbol{\lambda}$ are iteratively obtained. For instance, the design variables $t_i^*$ replaced by the design variables $t_i$ in the previous iteration are substituted into Eq. (37) to obtain *D* and *H*. Then $\boldsymbol{\lambda}$ can be obtained by solving the quadratic programming model (36). Finally, $t_i^*$ can be obtained from Eq. (30).

## 4. Numerical examples

This section illustrates the proposed approach with four numerical examples which include

under a single load case and multiple load cases. For simplicity, all the quantities are dimensionless. In addition, Young's modulus is chosen as $2.1\times10^{11}$ and Poisson's ratio as 0.3 for all examples. The scale parameter $r_{\min} = 1.5d$ is selected where $d$ denotes the length of the element diagonal. All finite element analyses are carried out using the commercial software package, ABAQUS.

### *4.1 L-bracket*

Fig. 2 shows the design domain of L-bracket which is fixed at the upper end and a concentrated force P = 4000 is applied downward at the point A. The thickness of the L-bracket is 0.5. The initial vertical displacement of the point A is $4.72\times10^{-5}$ downward. The displacement constraint, $1.0\times10^{-4}$ is specified at the point A in the vertical direction. The design domain is divided into a mesh with 1600 four-node plane stress elements. There are totally 1701 design variable points distributed within the design domain.

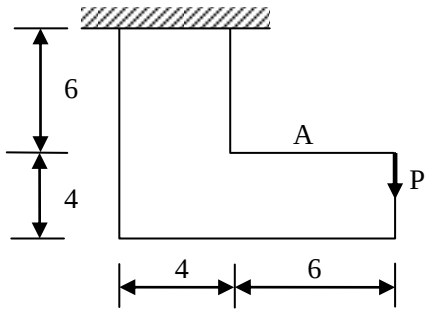


Fig. 2 The L-bracket design domain and its boundary condition

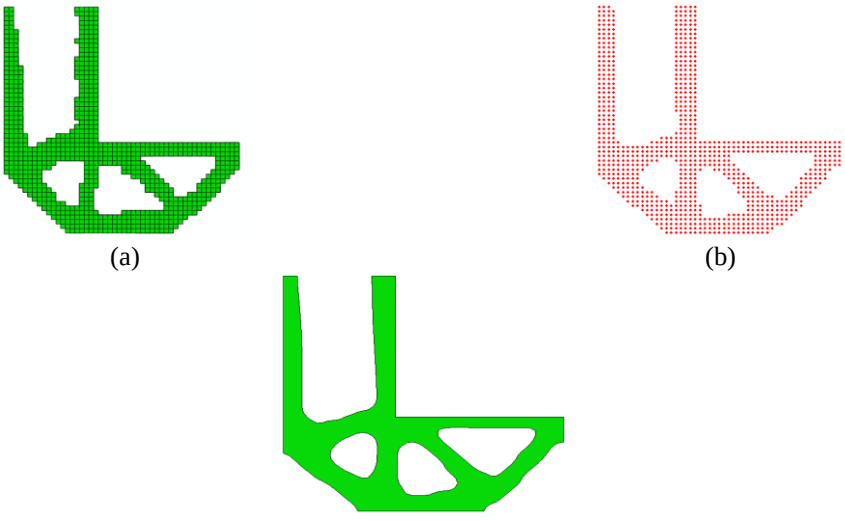

(a) (b)

(c)

Fig. 3 The L-bracket: (a) optimal topology obtained from the element-wise method; (b) material density distribution at the design variable points; (c) optimal topology obtained from EIND

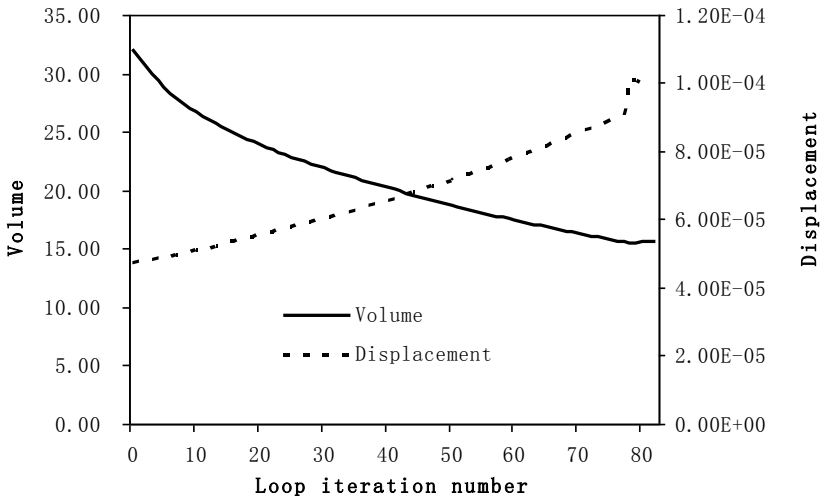


Fig. 4 The evolution histories of structural volume and displacement at point A of the L-bracket

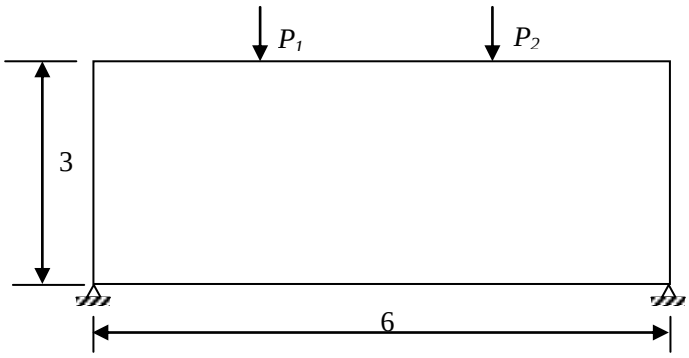


Fig. 5 The design domain and its boundary condition.

### *4.2 Multiple load cases and multiple displacement constraints*

Fig. 5 shows a design domain with length of 6, height of 3 and thickness of 0.2, which is fixed at two lower corners. Two load cases are specified with $P_1 = 4000$ for load case one and $P_2 = 4000$ for load case two. The design domain is divided into 60×30 four-node elements. There are 61×31 design variable points distributed within the design domain. The displacement constraints are applied at points where the forces are acted. The maximum displacements in both load cases at the constraint points are $9.007\times10^{-7}$ downward for the initial full design and their constraints are set to be $1.500\times10^{-6}$.

The optimal designs denoted by the material density at points and its contour are shown in Fig. 6. Once again, the proposed approach provides a clear and smooth topological contour. Figure 7 gives the evolution histories of the structural volume and the displacement constraints (note that the both displacement constraints are the same due to the symmetric nature of the problem). In this case, the objective function converges to the final value of 1.960 and the displacements are successfully constrained to the specified value, $1.500\times10^{-6}$ after the 53 iterations.

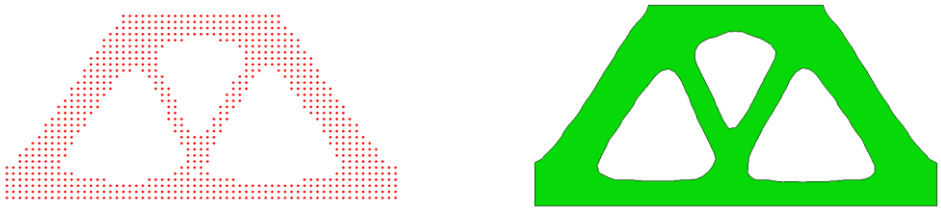

(a) (b)

Fig. 6 Topology optimization designs: (a) material density distribution at the design variable points; (b) optimal topology obtained from EIND

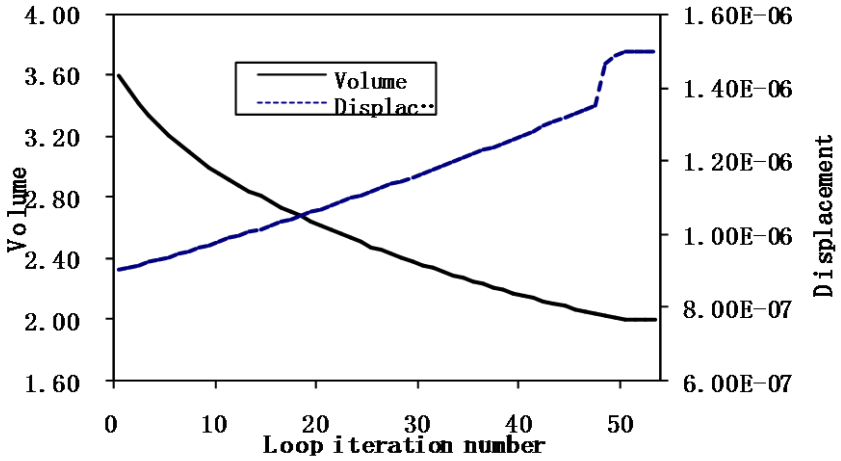


Fig. 7 The evolution histories of the structural volume and displacements at the constraints

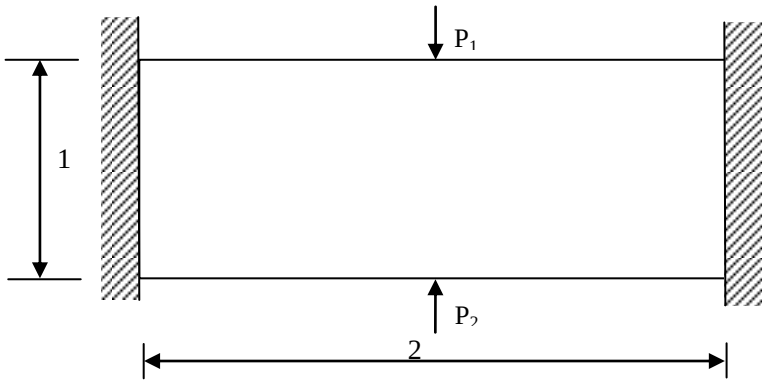


Fig. 8 The design domain and its boundary condition

Fig. 8 shows the rectangular design domain with width of 2, height of 1 which are fixed at the both ends. The uniform thickness of 0.1 is assigned for the whole design domain. The initial full design is divided into 40×20 four-node elements with 41×21 design variable points. In the load case one, $P_1 = 4000$ is acted downward at the middle of the top edge. In the load case two, $P_2 = 4000$ is acted upward at the middle of the bottom edge. The displacement constraints are applied at

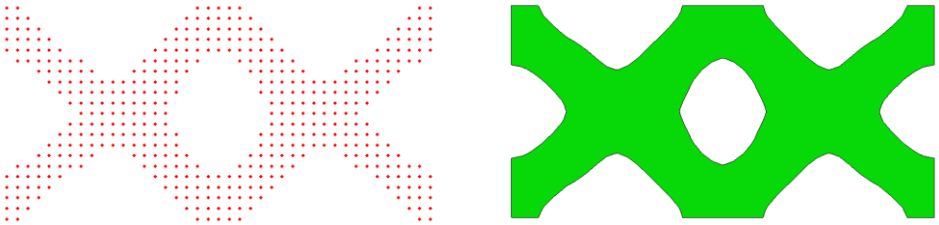

(a) (b)

Fig. 9 Topology optimization designs: (a) material density distribution at the design variable points; (b) optimal topology obtained from EIND

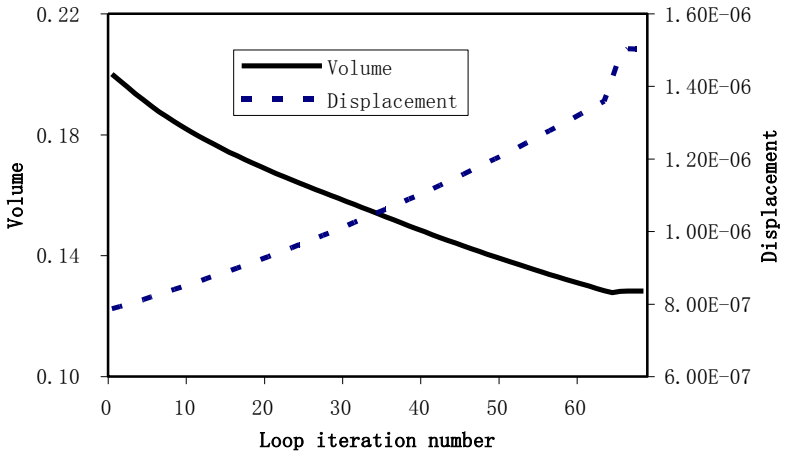


Fig. 10 The evolution histories of the structural volume and displacements at the constraints

the locations where the forces are acted. Both displacements at the constraint points for the initial full design are $5.846\times10^{-7}$, but one is downward and another is upward. The both constraint values are set to be $1.500\times10^{-6}$.

The volume optimization history of the structure above is presented in Fig. 10, and the displacement optimization history at the constraint point of the structure above is also depicted in Fig. 10. In this case, the objective function converges to the final value of 0.128 and the displacement constraint remains $1.500\times10^{-6}$ after the 66th iteration step.

The optimal design denoted by the densities at the design points is shown in Fig. 9(a) and its contour obtained from element independent nodal density is shown in Fig. 9(b). The contour gives the clear and smooth optimal design without any checkerboard pattern. Figure 10 shows the evolution histories of the structural volume and the displacements at the constraint points. After 66 iterations, the structural volume converges to its final value of 0.128 and both displacements converge to their constraint values $1.500\times10^{-6}$.

When the same mesh is used, computational cost for the topology optimization based on element independent nodal density is higher than the element-based approach. This mainly attributes to the large number of density nodes in the influence domain. However, the topology

resolution resulting from the proposed approach based on EIND is higher than that of the element-based approach. To improve the efficiency of the proposed approach especially for a 3D large-scale optimization problem, the parallel programming technique will be used to carry out the finite element analysis in the next example.

### *4.3 A cubic block*

Now that all commercial processors have become multi-cores, OpenMP can provide one of the few programming models that allow users to easily carry out the parallel computation of these processors. Even with multiple slow cores, it is still possible to achieve higher computational efficiency than that using a super-fast single processor (Chapman *et al.* 2007). Nowadays personal computers using the multi-core processing technology become widely available to consumers. In order to use a multi-core processor at full capacity, a new multi-thread code is programmed and run on a multi-core system. Such improvements will provide a faster solution for the following 3D example.

A cubic domain shown in Fig. 11(a) is divided into mesh size of 40×40×40 eight-node elements. Two load cases are considered with $P_1$ = 4,000 and $P_2$ = 4,000 applied to the top face in the $y$ direction respectively. The four lower corners are fixed, as shown in Fig. 11(a). Three displacements at the locations of load $P_1$ and $P_2$ and the center of the top face are constrained to the given limits. The $y$ directional displacements at the locations of $P_1$ and $P_2$ for the initial full design are identical to be $8.944\times10^{-11}$, and their constraint values are taken as $1.5\times10^{-10}$. The $x$ directional displacement at the center of the top face for the initial full design is $7.524\times10^{-12}$, and its constraint value is taken as $1.0\times10^{-11}$.

The resulting optimal topology obtained from the NDEI approach is shown in Fig. 11(b). Numerical experience indicates that the parallel computational time is approximately three times shorter than that of the serial computation when the four-core processor was used, Although the computational efficiency does not increase proportional to the number of the core, the parallel programming technique achieves adequate benefit in term of the computation time especially when the number of design variables increases. The use of parallel programming technique has also been reported to achieve high computational efficiency (Colominas *et al.* 2009) but it only requires an acceptable additional programming effort when OpenMP directives are used.

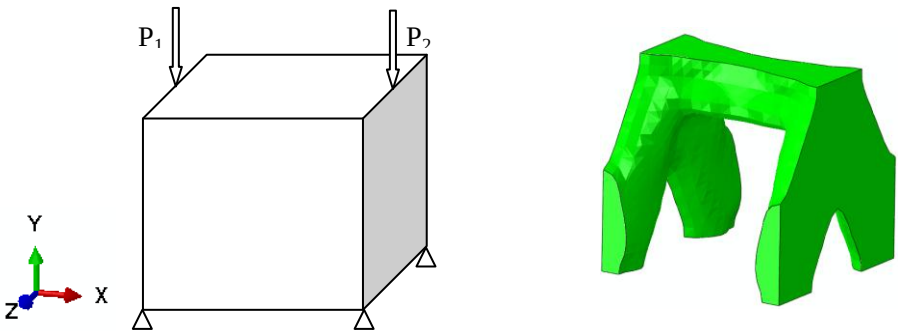


(a) (b)

Fig. 11 (a)The 3D design domain and its boundary condition; (b) Optimal topological design

## 5. Conclusions

This paper has considered the topology optimization problem which minimizes the volume of the structure subject to multiple displacement constraints under multiple load cases. A topology optimization method has been developed using element independent nodal density values as design variables. Traditionally a constant element density within a finite element is used. In contrast to the element-based procedure, point density values are interpolated by Shepard function and the Heaviside function in this paper to avoid checkerboard patterns and mesh-dependency for the low order finite elements. Sequential quadratic programming algorithm and dual programming are employed with an iterative scheme for updating the design variables. Finally, almost black and white design can be obtained based on the point densities. These density values are further to determine a smooth iso-line/surface to describe the boundary of the optimal layout. As a result, a smooth optimal topology is obtained.

Numerical examples demonstrate the effectiveness of the proposed method based on EIND to obtain optimal solutions by comparing with the typical solutions of element-based topology optimization. The numerical results also indicate that the numerical instability problems related to a finite element mesh are successfully overcome by the proposed method. Furthermore, the multi-thread parallel computation technique with OpenMP has been implemented so that the computational efficiency has significantly improved especially for the 3D optimization problem.

## Acknowledgements

This work has been supported by the National Natural Science Foundation of China (10872036), the High Technological Research and Development Program of China (2008AA04Z118), Natural Science Foundation Collaborative Research Grant for Overseas, Hong Kong and Macau Scholars (51228801), Hunan Provincial Natural Science Foundation of China (12JJ3044), the Huxiang Scholar funding from Changsha University of Science and Technology and the Furong Scholar funding from Hunan Province，the Key Laboratory of Lightweight and Reliability Technology for Engineering Vehicle, Education Department of Hunan Province (Changsha University of Science & Technology)(2012KFJJ02).

## References

Beckers, M. (1999), "Topology optimization using a dual method with discrete variables", *Struct. Optim.*, **17**(1), 14-24.

Bendsøe, M.P. and Kikuchi, N. (1988), "Generating optimal topologies in structural design using a homogenization method", *Comput. Meth. Appl. Mech. Eng.*, **71**(2), 197-224.

Bendsoe, M.P. (1989), "Optimal shape design as a material distribution problem", *Struct. Multidisc. Optim.*, **1**(4), 193-202.

Bendsøe, M.P. and Sigmund, O. (2003), *Topology Optimization: Theory, Methods, and Applications*. Springer-Verlag, New York, USA

Brodlie, K.W., Asim, M.R. and Unsworth, K. (2005), "Constrained visualization using the shepard interpolation family", *Comput. Graphics Forum*, **24**(4), 809-820.

Carbonari, R.C., Silva, E.C.N. and Nishiwaki, S. (2004), "Topology optimization applied to the design of multi-actuated piezoelectric micro-tools", *Smart Structures and Materials 2004: Modeling, Signal*

*Processing, and Control (Proceedings of SPIE)*, San Diego, USA, March.
Chapman, B., Jost, G. and Pas, R.V.D. (2007), *Using OpenMP: Portable Shared Memory Parallel Programming*, The MIT Press, Cambridge, Massachusetts, USA.
Colominas, I., Parıs, J., Navarrina, F. and Casteleiro, M. (2009), "High performance parallel computing in structural topology optimization", *Proceedings of the 12th International Conference on Civil, Structural and Environmental Engineering Computing*, Funchal, Portugal, September.
Diaz, A. and Sigmund, O. (1995), "Checkerboard patterns in layout optimization", *Struct. Optim.*, **10**(1), 40-45.
Guest, J.K., Prevost, J.H. and Belytschko, T. (2004), "Achieving minimum length scale in topology optimization using nodal design variables and projection functions", *Int. J. Numer. Meth. Eng.*, **61**(2), 238-254.
Huang, X. and Xie, Y. (2007), "Convergent and mesh-independent solutions for the bi-directional evolutionary structural optimization method", *FINITE ELEM. ANAL. DES.*, **43**(14), 1039-1049.
Huang, X. and Xie, Y.M. (2010), *Evolutionary Topology Optimization of Continuum Structures: Methods and Applications*, John Wiley & Sons, Chichester, West Sussex, UK.
Jog, C.S. and Haber, R.B. (1996), "Stability of finite elements models for distributed-parameter optimization and topology design", *Comput. Meth. Appl. Mech. Eng.*, **130**(3-4), 203-226.
Kang, Z. and Wang, Y.Q. (2011), "Structural topology optimization based on non-local Shepard interpolation of density field", *Comput. Meth. Appl. Mech. Eng.*, **200**(49-52), 3515-3525.
Lee, D.K. (2007), "Combined topology and shape optimization of structures using nodal density as design parameter ", *J. ASIAN. ARCHIT. BUILD.*, **6**(1), 159-166.
Lee, D.K., Kim, J.H., Starossek, U. and Shin, S.M. (2012), "Evaluation of structural outrigger belt truss layouts for tall buildings by using topology optimization", *Struct. Eng. Mech.*, **43**(6), 711-724.
Lee, E.H. and Park, J. (2011), "Structural design using topology and shape optimization", *Struct. Eng. Mech.*, **38**(4), 517-527.
Matsui, K. and Terada, K. (2004), "Continuous approximation of material distribution for topology optimization", *Int. J. Numer. Meth. Eng.*, **59**(14), 1925-1944.
Paulino, G.H. and Le, C.H. (2009), "A modified Q4/Q4 element for topology optimization", *Struct. Multidisc. Optim.*, **37**(3), 255-264.
Poulsen, T.A. (2002), "Topology optimization in wavelet space", *Int. J. Numer. Meth. Eng.*, **53**(3), 567-582.
Rahmatalla, S.F. and Swan, C.C. (2004), "A Q4/Q4 continuum structural topology optimization implementation", *Struct. Multidisc. Optim.*, **27**(1), 130-135.
Rong, J.H., Li, W.X. and Feng, B. (2010), "A structural topological optimization method based on varying displacement limits and design space adjustments", *Adv. Mater. Res.*, **97-101**, 3609.
Rong, J.H. and Liang, Q.Q. (2008), "A level set method for topology optimization of continuum structures with bounded design domains", *Comput. Meth. Appl. Mech. Eng.*, **197**(17-18), 1447-1465.
Rozvany, G.I.N. (2001), "Aims, scope, methods, history and unified terminology of computer-aided topology optimization in structural mechanics", *Struct. Multidisc. Optim.*, **21**(2), 90-108.
Rozvany, G.I.N., Zhou, M. and Birker, T. (1992), "Generalized shape optimization without homogenization", *Struct. Multidisc. Optim.*, **4**(3-4), 250-254.
Sethian, A. and Wiegmann, A. (2000), "Structural boundary design via level set and immersed interface methods", *J. Comput. Phys.*, **163**(2), 489-528.
Shepard, D. (1968), "A two-dimensional interpolation function for irregularly-spaced data", *Proceedings of the 1968 23rd ACM National Conference*, New York, January
Sigmund, O. and Petersson, J. (1998), "Numerical instabilities in topology optimization: a survey on procedures dealing with checkerboards, mesh-dependencies and local minima", *Struct. Optim.*, **16**(1), 68-75.
Stolpe, M. and Svanberg, K. (2001), "An alternative interpolation scheme for minimum compliance topology optimization", *Struct. Multidisc. Optim.*, **22**(2), 116-124.
Swan, C.C. and Kosaka, I. (1997), "Voigt-Reuss topology optimization for structures with linear elastic material behaviours", *Int. J. Numer. Meth. Eng.*, **40**(16), 3033-3057.

Wang, M.Y., Wang, X.M. and Guo, D.M. (2003), "A level set method for structural topology optimization", *Comput. Meth. Appl. Mech. Eng.*, **192**(1), 227-246.
Xie, Y.M. and Steven, G.P. (1993), "A simple evolutionary procedure for structural optimization", *Comput. Struct.*, **49**(5), 885-896.
Xie, Y.M. and Steven, G.P. (1997), *Evolutionary Structural Optimization*. Springer, Berlin, Germany.
Yang, R.J. and Chuang, C.H. (1994), "Optimal topology design using linear programming", *Comput. Struct.*, **52**(2), 265-275.